nature nanotechnology

LETTERS

PUBLISHED ONLINE: 19 APRIL 2009 | DOI: 10.1038/NNANO.2009.81

# The crossover from two dimensions to one dimension in granular electronic materials

Ke Xu†, Lidong Qin† and James R. Heath*

**Granular conductors[1] are solids comprising densely packed nanoparticles, and have electrical properties that are determined by the size, composition and packing of the composite nanoparticles. The ability to control these properties in two- and three-dimensional granular conductors has made such systems appropriate for use as prototypes for investigating new physics[1–4]. However, the fabrication of strictly one-dimensional granular conductors remains challenging. Here, we describe a method for the assembly of nanoparticles into granular solids that can be tuned continuously from two to one dimension, and establish how electron transport evolves between these limits. We find that the energy barriers to transport increase in the one-dimensional limit, in both the variable-range-hopping (low-voltage) and sequential-tunnelling (high-voltage) regimes. Furthermore, in the sequential-tunnelling regime we find an unexpected relationship between the temperature and the voltage at which the conductance becomes appreciable — a relationship that appears peculiar to one-dimensional systems. These results are explained by extrapolating existing granular conductor theories to one dimension.**

A particularly rich area of nanoscale science is the investigation of low-dimensional systems, such as two-dimensional thin films, one-dimensional nanowires and zero-dimensional quantum dots[2,5–7]. In such systems, the electronic structure of the material and the statistical distribution of charge transport pathways are strongly influenced by dimensionality. An equally rich area, but one that is more difficult to investigate, is the physics associated with dimensional crossover. Granular conductors[1], in principle, provide the flexibility for investigating such crossovers. This is because the constituent nanoparticle properties[8] are independent of how they are assembled. Indeed, granular materials self-assembled from monodisperse, chemically synthesized colloidal quantum dots (QDs)[2,5,6] into highly ordered three- and two-dimensional architectures[2–4] have provided a laboratory for investigating new physics, including, for instance, the long-range resonance transfer of electronic excitations in three-dimensional QD solids[2] and the metal-to-insulator transition in two-dimensional QD superlattices[3]. In contrast, attempts to assemble nanoparticles into ordered one-dimensional (single-file nanoparticle arrays/chains) or quasi-one-dimensional granular structures have only achieved limited success[9–14], largely due to the difficulty in obtaining continuously connected one-dimensional superstructures.

We used a template-directed approach to align QDs into densely packed one-dimensional superstructures, using surface interactions between nanopatterned substrates and QD solutions. Similar methods have been used to fabricate ordered nano/microsphere assemblies over particle sizes ranging from micrometres to 50 nm (refs 15–17). In this study, ordered QD one-dimensional assemblies were achieved by precisely controlling the widths of nanopatterned one-dimensional trenches (the templates) to within ~1 nm, using QDs characterized by a narrow size distribution and controlling the QD/trench chemical interface.

Arrays of $SiO_2$ nanotrenches were fabricated using superlattice nanowire pattern transfer[18], which translates atomic control over the film thicknesses within a $GaAs/Al_xGa_{1-x}As$ superlattice into control over the width and spacing of nanotrenches. The nanotrench surfaces were chemically functionalized with hexamethyldisilazane. The resultant hydrophobic substrate was dip-coated in a toluene solution of QDs (Fig. 1a, b). A wetting meniscus was formed in the process.

Closest-packed QDs fill the nanotrenches (Fig. 1c–f). Figure 1c shows the fidelity of this technique: well-ordered, 3-QD-wide, closest-packed structures are observed in each of the nanotrenches, with lengths of up to 1 mm. The QD solution coats the entire wafer during dip-coating, but only leaves a single layer of QDs deposited within the trenches—a result that likely arises from the increased QD/surface interactions within the trenches. The packing pattern can be fine-tuned by either adjusting the trench width (Fig. 1c–f) or the size or shape of the QD (see Supplementary Information). For each of the arrays reported here, the dipping rate was also an important and separately optimized parameter. The technique works well for trench widths of $\geq$5 nm (see Supplementary Fig. S1).

The assembly method typically generates >100 identically packed parallel QD arrays. This enabled us to sample a statistically relevant number of QD arrays for each of the transport measurements reported here. The insulating $SiO_2$ trench walls prevent electrical crosstalk between adjacent QD arrays. Magnetite QDs, used as our model system, are half-metallic, and strong magnetoresistance effects have been reported[19].

To characterize how the two-dimensional → one-dimensional crossover influences the electrical properties of granular electronic systems, we investigated a single QD size (15 nm) and varied the trench widths to control the number of QDs across the width of each array. Quasi-one-dimensional arrays with 3 (Fig. 1c), 2 (Fig. 1e) and 1.5 (zigzag structure, Fig. 1f) QDs across the width, as well as one-dimensional linear arrays (Fig. 1d) were studied and compared with a close-packed QD monolayer film. Other research groups have found that quasi-one-dimensional QD arrays as narrow as four-QD wide are electronically similar to full two-dimensional arrays[11].

We fabricated about 50 devices, each contacting 50 to 400 parallel, identically packed one-dimensional or quasi-one-dimensional arrays (Fig. 2a), and plotted the measured resistance per array as a function of array length (see Supplementary Information). A linear dependence is observed, indicating that the device transport properties are dominated by the QD arrays, with negligible contribution from contacts. Owing to the large number of parallel channels, defects such as missing particles are not expected to affect the measurements at the array lengths reported here. Large negative magnetoresistance were found for all devices, verifying that the

Kavli Nanoscience Institute and Division of Chemistry and Chemical Engineering, California Institute of Technology, MC 127-72, Pasadena, California 91125, USA; †These authors contributed equally to this work. *e-mail: heath@caltech.edu

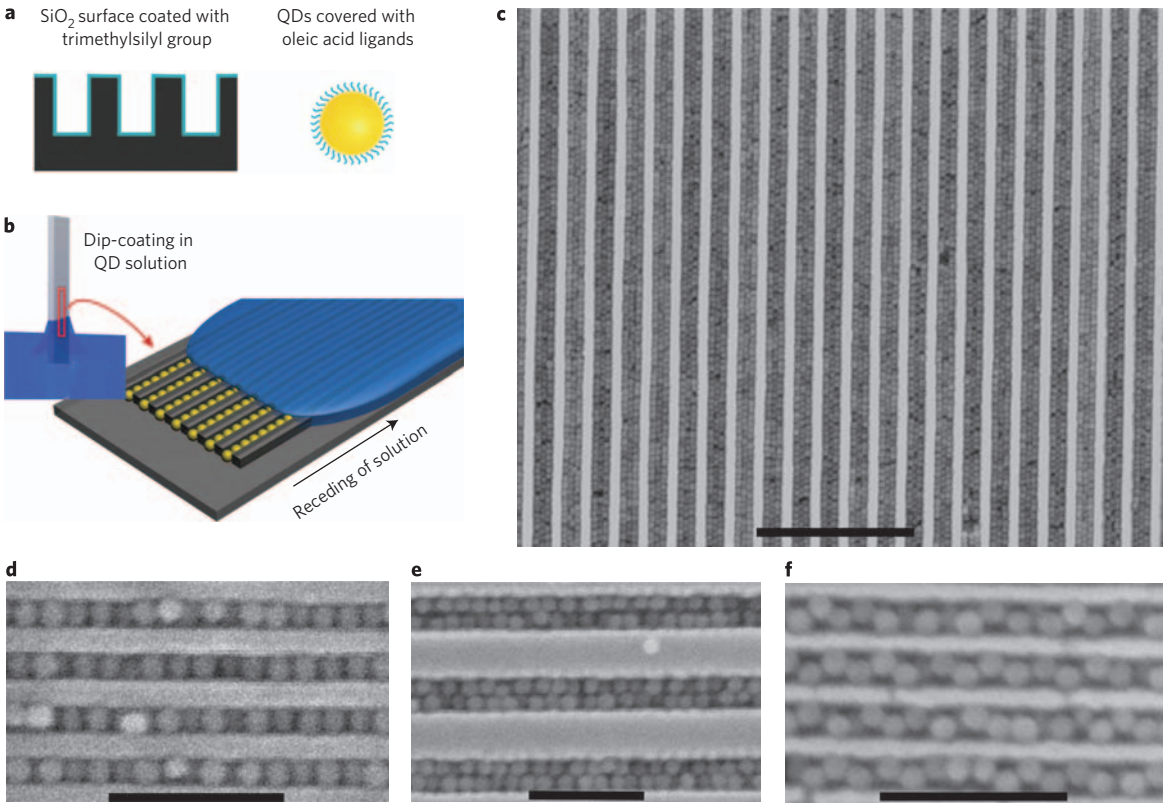


**Figure 1 | Assembling QDs into one-dimensional and quasi-one-dimensional arrays. a**, Surface functionalization of silica nanowire/nanotrench arrays (left) and a schematic of a QD and its surface ligands (right). **b**, Dip-coating method to fabricate QD arrays: one-dimensional QD arrays are formed as the QD solution recedes along the nanotrench substrate. **c–f**, SEM images of 3-line (**c**), 1-line (**d**), 2-line (**e**) and 1.5-line (**f**) (zigzag) QD arrays of 15 nm magnetite QDs. Scale bars, 400 nm (**c**), 100 nm (**d–f**).

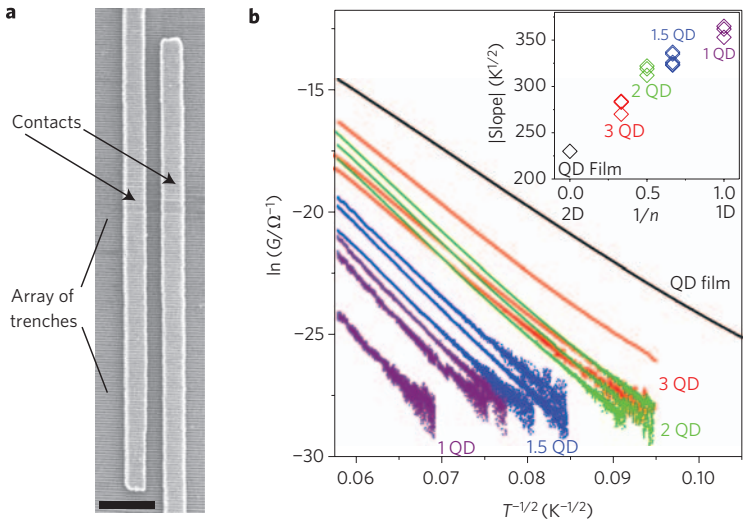


**Figure 2 | Conductance measurement of the QD arrays. a**, SEM image of a typical device used for the electrical measurements, which contacts 160 parallel one-dimensional QD arrays. Scale bar, 1 μm. **b**, Temperature-dependent conductance at low voltage bias. The number of QDs across the width of each array is indicated. One-dimensional zigzag arrays are labelled as 1.5 QD. Inset: $\ln(G)$–$T^{-1/2}$ slopes of the QD arrays plotted as a function of the dimensionality of the system, where $n$ is the number of QDs across the width of each array.

measured electrical properties arise from the magnetite QD arrays (see Supplementary Information).

The conductance $G$ of the QD arrays was studied at low (<100 mV) applied voltage bias as a function of temperature $T$ (Fig. 2b). A linear dependence was found for all arrays when $G$ was plotted on a logarithmic scale against $T^{-1/2}$, in agreement with previous studies on two- and three-dimensional QD assemblies[19–23]. Such behaviour is commonly ascribed[20–23] to the Efros–Shklovskii variable-range hopping (ES-VRH)[24] (or super-exchange[25]) transport mechanisms, although recent studies have also suggested alternative

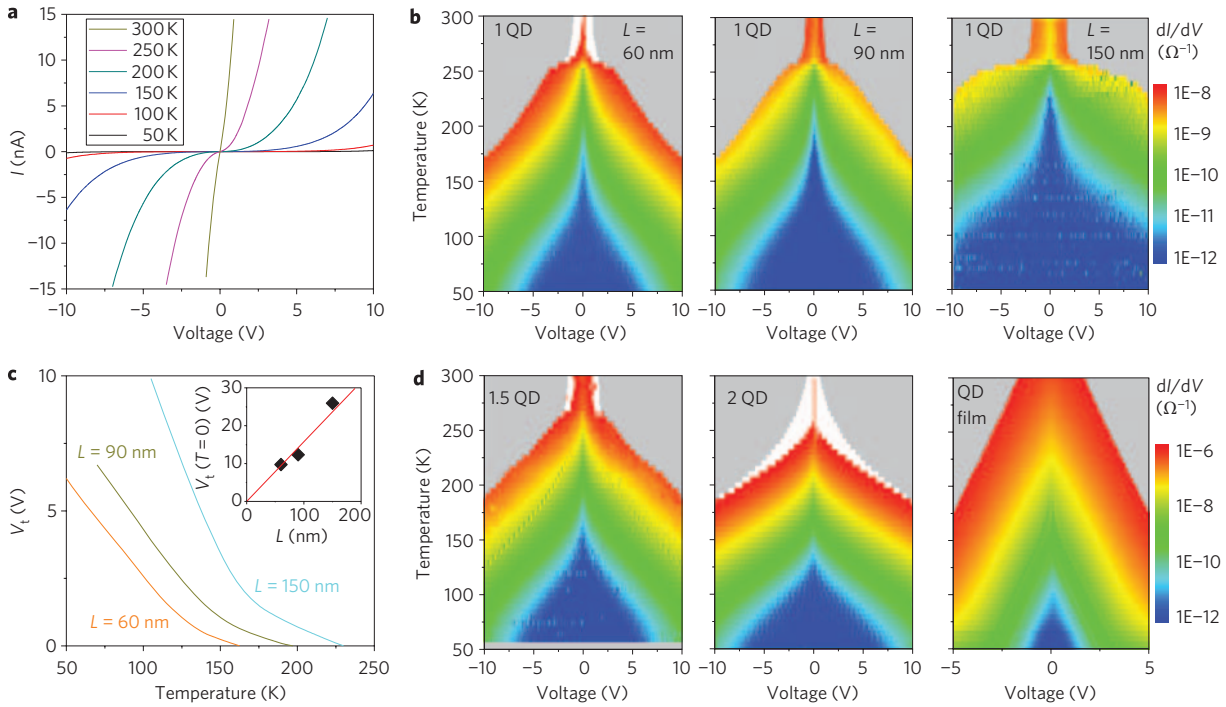


**Figure 3 | Electrical properties of the QD arrays at high voltage. a**, *I–V* curves of a QD one-dimensional linear array device at various temperatures. **b**, Differential conductance (d*I*/d*V*) as a function of voltage and temperature for one-dimensional linear arrays with various lengths. White areas indicate regions in which the differential conductance is higher than the upper limit of the colour scale. Grey areas indicate unmeasured regions in which the current level would be higher than the upper compliance of current (~20 nA) set to protect the devices. **c**, Threshold voltage as a function of temperature for the three devices in **b**. Inset: extrapolated threshold voltage at 0 K as a function of length. **d**, Differential conductance as a function of voltage and temperature for a one-dimensional zigzag QD array device, a quasi-one-dimensional device with two QDs across the width of each array, and a two-dimensional QD monolayer film. The colour scale shown in **b** applies to the one-dimensional zigzag and quasi-one-dimensional devices, whereas the expanded scale in **d** applies for the QD film device. Grey areas indicate unmeasured regions.

mechanisms[1,23] such as elastic and inelastic co-tunnelling[1]. We use the ES-VRH model to explain our data because that model has been the most widely used and permits the broadest comparison of our results against the literature.

Precisely controlled assembly helps to reveal trends in our $G$–$T$ data: similar $\ln(G)$–$T^{-1/2}$ slopes were found for devices with the same designed numbers of QDs across the width of each array (see Supplementary Information for the consistent slopes obtained on five different one-dimensional zigzag array devices), whereas notably (up to ~60%) steeper slopes were observed as the QD assemblies cross over from two to one dimension (Fig. 2b, inset).

The results presented in Fig. 2 indicate an increasing energy barrier for charge transport accompanies the two- to one-dimensional crossover. According to VRH, charge transport efficiency is determined by the optimal hopping network, which in turn is determined by competition between the hopping distance and the number of available energy levels at a given distance. ES-VRH predicts a linear $\ln(G)$–$T^{-1/2}$ relationship[24]:

$$G(T) \sim \exp[-(T_0/T)^{1/2}],\ T_0 = \beta_D e^2/\kappa a \qquad (1)$$

where $e$ is the electron charge, $\kappa$ is the dielectric constant, and $a$ is the localization length, which characterizes the decay length of electronic wavefunctions and in QD arrays is approximately the size of each QD (refs 21,22). The coefficient $\beta_D$ depends on the system dimensionality $D$, and should increase as $D$ is reduced; establishing a (percolating) hopping network becomes increasingly difficult with reducing dimensions, and so the energy barrier for conductance is higher. For three- and two-dimensional cases, theory and simulations indicate[26,27] that $\beta_3 \approx 2.8$ and $\beta_2 \approx 6.5$. No theoretical investigation of $\beta_1$ has been reported. Our data allow for an experimental determination of $\beta_1$. The consistent trend of the $\ln(G)$–$T^{-1/2}$ slopes suggests that $\beta_D$ increases progressively as the array evolves from two to one dimension. For one-dimensional linear arrays, the absolute value of the $\ln(G)$–$T^{-1/2}$ slope increases to 360 $K^{1/2}$ from 230 $K^{1/2}$ in two dimensions. Consequently, assuming similar localization lengths for one- and two-dimensional arrays, this suggests $\beta_1/\beta_2 \approx (360/230)^2 = 2.45$ and $\beta_1 \approx 16$. This result is plausible, considering that a 2.3-fold (6.5/2.8) increase in $\beta_D$ is found for two-dimensional systems when compared to three-dimensional systems.

At low temperatures, conductance due to the thermally activated hopping processes falls below the detection limit at low bias voltages. On the other hand, high bias voltages can overcome the Coulomb blockade and result in measurable conductance through sequential tunnelling between nearest-neighbour particles. This different mechanism of conductivity should yield different dimensional/geometric effects.

Figure 3a presents the *I–V* curves measured on a one-dimensional linear QD array device at different temperatures. As the temperature is lowered from room temperature, a gap of low current opens up at low voltages[10,23,28,29], and a finite threshold voltage $V_t$ is required for the onset of appreciable ($>5 \times 10^{-12}\ \Omega^{-1}$) conductance. To further characterize how the electrical properties evolve for all temperatures, we present in Fig. 3b the differential conductance d$I$/d$V$ measured on three one-dimensional linear array devices as a function of both $V$ and $T$, from which the $V_t$–$T$ relationship can be readily identified (Fig. 3c).

$V_t$ is found to be directly proportional to the length of the assembly, $L$, both for one-dimensional linear arrays (Fig. 3c) and zigzag arrays (see Supplementary Information). This result was predicted[30,31]: $V_t$, the overall energy barrier for charge transport, is proportional to the

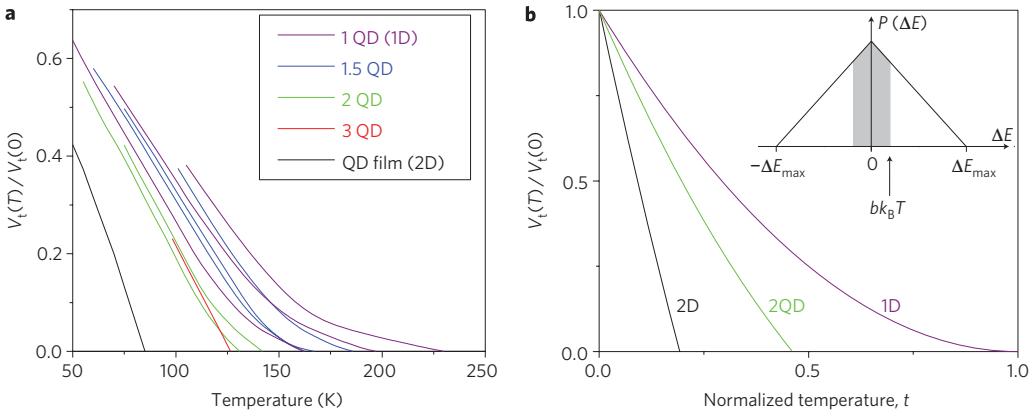


**Figure 4 | Temperature dependence of the threshold voltage. a**, Experimental threshold voltage–temperature dependence measured on different QD array devices. The threshold voltages are normalized to the extrapolated values at 0 K. The number of QDs across the width of each array is indicated in the graph. One-dimensional zigzag arrays are labelled as 1.5 QD. **b**, Theoretical threshold voltage–temperature dependence. Black and purple lines represent the two- and one-dimensional cases, respectively. The green line represents an intermediate case with $p_c = 0.71$, corresponding to 2-QD-wide quasi-one-dimensional arrays (see Supplementary Information). $t$ is the normalized temperature, where $t = bk_BT/\Delta E_{max}$. Inset: probability distribution for $\Delta E$ in tunnelling events.

number of tunnelling barriers in the conduction path, which is in turn proportional to $L$. This contrasts with the low-voltage VRH conductance, in which the relevant energy barrier for charge transport ($T_0$) only depends on the localization length and the dimensionality of the system (equation (1)). As a result, similar $\ln(G)$–$T^{-1/2}$ slopes are found for different devices with the same numbers of QDs across the width of each array, regardless of $L$ (Fig. 2b).

For the one-dimensional arrays, a linear $V_t$–$T$ relationship is observed at low $T$, but at high $T$ and low $V$, a pronounced sublinear $V_t$–$T$ relationship is found (Fig. 3b,c). This indicates that more thermal energy is required to overcome the remaining energy barriers for charge transport. Linear $V_t$–$T$ relationships have been observed previously up to the temperature where $V_t$ drops to zero in two-dimensional QD assemblies[28,29] and quasi-one-dimensional chains of irregular nanoparticles[10], and has been explained by theory[31,32]. The sublinear $V_t$–$T$ relationship we find has neither been predicted nor observed previously. Our results (Figs 3b–d,4a) indicate that this phenomenon is peculiar to one-dimensional QD arrays: the sublinearity is pronounced in both the one-dimensional linear and zigzag arrays, barely seen in 2-QD-wide quasi-one-dimensional arrays, and not observed at all in wider quasi-one-dimensional QD arrays or two-dimensional QD films.

This novel sublinear $V_t$–$T$ relationship can be explained by extrapolating the theoretical discussions of Jaeger and colleagues[29,31]. Consider the case when the coupling capacitance between QDs is negligible compared to $C_0$, the capacitance of an individual QD. When an electron tunnels from a QD to its nearest neighbour, the energy change for the system, $\Delta E$, falls into the range $[-\Delta E_{max}, \Delta E_{max}]$, where $\Delta E_{max} = e^2/C_0$, and a triangle-shaped distribution of the probability density, $P(\Delta E)$, is expected (Fig. 4b, inset)[29]. A finite temperature broadens the energy levels of the QDs, and conduction barriers are removed for neighbouring QDs satisfying $|\Delta E| < bk_BT$, where $b \approx 2.4$ characterizes the extent of thermal broadening of the Fermi–Dirac distributions in QDs (ref. 31). When the fraction of conduction barriers being removed, $p(T)$, reaches the bond percolation threshold of the lattice, $p_c$, a continuous path with all barriers removed emerges, and $V_t(T)$ drops to zero. The $V_t$–$T$ relationship is thus modelled as[31] $V_t(T)/V_t(0) = 1 - p(T)/p_c$.

Previous studies[29,31] have considered the two-dimensional case, where $p_c \approx 0.347$ is small due to the existence of multiple possible pathways. Only 34% of all the conduction barriers need to be overcome for $V_t(T)$ to drop to 0 (the shaded area in Fig. 4b inset). In this region, $P(\Delta E)$ is effectively constant, so the same increment of temperature results in the removal of the same number of conductance barriers. As a result, a linear $V_t$–$T$ relationship is observed.

By contrast, one-dimensional lattices have only a single pathway available for tunnelling conductance ($p_c = 1$), and so every tunnel barrier must be overcome for current to flow. Because $P(\Delta E)$ is considerably smaller for larger $|\Delta E|$, smaller numbers of barriers are removed for an equal temperature increase at higher $T$. In particular, because $P(\Delta E)$ drops towards zero when $|\Delta E|$ approaches $\Delta E_{max}$, the last small fraction of barriers that keep $V_t$ from dropping to zero are especially difficult to overcome. This explains the sublinear dependence of $V_t$ on $T$ we find at high temperature and low bias.

By integrating $P(\Delta E)$ from $-bk_BT$ to $bk_BT$, we have plotted the theoretical $V_t$–$T$ relationship (Fig. 4b). The results satisfactorily capture our experimental data (Fig. 4a) for the two- and one-dimensional cases, and support our observation that the sublinearity is peculiar to truly one-dimensional QD arrays: $p_c$ drops rapidly below 1 for quasi-one-dimensional arrays; for 2-QD-wide arrays, $p_c \approx 0.71$, and the sublinearity becomes much less noticeable (Fig. 4b).

Similar $V_t$–$T$ behaviours were observed for one-dimensional linear and zigzag arrays, because they are topologically equivalent for percolation in the tunnelling regime; that is, each QD has two nearest neighbours for charge tunnelling. In contrast, in the VRH regime, the zigzag arrangement allows for an increase in the density of hopping pathways, and therefore appreciably smaller $\beta_D$ and $\ln(G)$–$T^{-1/2}$ slopes are found relative to the linear arrangement (Fig. 2b, inset).

The described approach for assembling arrays of monodisperse QDs permits the electron transport properties of granular systems to be characterized across the two- to one-dimensional crossover. The electrical properties of one-dimensional granular systems are significantly different from two-dimensional systems, due to the single available transport pathway in one dimension. Harnessing related approaches to characterize other, equally rich transport phenomena such as thermal conductance represents an exciting future challenge.

## Methods

**$SiO_2$ superlattice nanowire pattern transfer nanotrench array preparation.** An array of platinum superlattice nanowire pattern transfer (SNAP) nanowires was obtained by electron-beam evaporation onto the raised edges of a differentially etched edge of a epitaxially grown GaAs/$Al_xGa_{(1-x)}As$ superlattice wafer (IQE) (ref. 18). In this way, atomic control over the epilayer thicknesses of the superlattice stack was translated into control over the width and spacing of nanowires. The array of platinum SNAP nanowires was then transferred as an ink onto a 300-nm-thick, thermally grown $SiO_2$ layer on top of a silicon substrate. A thin (~10 nm) layer of heat-curable epoxy (EpoxyBond 110, Allied High Tech) was used to securely bond the platinum nanowire array to the surface. The superlattice/nanowire

array/epoxy/$SiO_2$ substrate assembly was baked on a hot plate at 150 °C for 15 min, and the superlattice was then released by a wet etch in a $H_3PO_4/H_2O_2/H_2O$ (5:1:50 v/v, 4.5 h) solution, leaving a highly aligned array of platinum nanowires on the surface of the $SiO_2$ substrate. The platinum nanowire array served as the protective mask for a reactive ion etch (RIE) process to produce a highly ordered $SiO_2$ nanowire/nanotrench array. A highly directional, 40 MHz Unaxis SLR parallel-plate RIE system was implemented to produce 50-nm-deep trenches in $SiO_2$ using $CF_4$/He (20/30 s.c.c.m., 5 mtorr, 40 W). The platinum nanowires were then dissolved in aqua regia (3:1 HCl:$HNO_3$) at boiling temperature for 30 min. The wafer was then rinsed with water and dried with a nitrogen blow, and heated in PRX-127 (Rohm & Haas LLC) to remove residual epoxy and other possible organic contaminants. Eventually, a highly ordered, ultrahigh-density array of $SiO_2$ nanowires/nanotrenches was obtained with a clean surface. The width of each nanowire is controlled by the thickness of the $Al_xGa_{(1-x)}As$ epilayers in the starting superlattice wafer, while the width of each nanotrench is controlled by the thickness of the GaAs epilayers. The number of nanowires/nanotrenches in the array is controlled by the number of epilayers in the superlattice wafer.

**Superlattice nanowire pattern transfer nanotrench array surface functionalization.** The as-prepared nanotrench array wafer was heated in a piranha solution (3:1 $H_2SO_4$:$H_2O_2$) at 120 °C for ~10 min, rinsed with water, and dried on a hot plate at 160 °C. The wafer was then surface-functionalized by exposure to a hexamethyldisilazane (Sigma-Aldrich) vapour within a sealed chamber. The resulting hydrophobic substrates formed a wetting meniscus contact with a toluene solution of QDs.

**Quantum dot solution preparation.** QDs covered with oleic acid ligands were used in this study. All the magnetite QD solutions were purchased from Ocean Nanotech. For the 15-nm QDs, the as-purchased chloroform solution (48 mg $ml^{-1}$) was diluted 40 times with toluene for a final concentration of 1.2 mg $ml^{-1}$. The diluted QD solution appeared dark grey and QDs were completely dispersed without any precipitates. The 25 and 40 nm magnetite QD solutions were prepared with the same protocol to a concentration of 1.5 and 2.0 mg $ml^{-1}$, respectively. Gold QDs (5 nm, from Xingchen Ye in the Christopher Murray Lab at the University of Pennsylvania), were dissolved in toluene to a final concentration of 5.0 mg $ml^{-1}$.

**Assembling quantum dots into nanotrench arrays.** The QD assembly step was performed by dip-coating a surface-functionalized $SiO_2$ nanotrench array wafer in a toluene solution of QDs. The wafer, clamped by a pair of tweezers and fixed onto a syringe pump (NE-1000 programmable syringe pump, New Era Pump Systems), was slowly withdrawn from the QD solution at a finely controlled speed (~0.5 mm $min^{-1}$) set to the gears of the pump. The speed was optimized for the formation of a close-packed monolayer inside each nanotrench (see Supplementary Information).

**Annealing of magnetite quantum dot arrays.** All assembled magnetite QD arrays were annealed to form a conductive phase[19]. The wafer with QD arrays was heated to 400 °C and annealed at this temperature for 60 min under the protection of ultrahigh-purity argon in a tube furnace (Linderberg, Model 54233), then cooled to room temperature overnight. The annealed QD arrays kept their original shape and arrangement as confirmed by scanning electron microscopy (SEM).

**Fabricating electrodes to contact the quantum dot arrays.** Metallic contact electrodes were patterned across the annealed QD arrays using electron-beam lithography. Two parallel electrodes (30-nm-thick titanium and 150-nm-thick gold), separated by a designed distance (from 50 to 500 nm), were precisely positioned across QD arrays according to alignment markers that were patterned on the wafer in an earlier step. The two electrodes were then connected to two large ($150 \times 150$ $\mu m^2$) gold pads from opposite directions (Fig. 2a), so the measured current was transmitted through a well-defined number of QD arrays. The pads were then wire-bonded to a chip carrier.

**Temperature- and magnetic-field-dependent electrical measurements.** All electrical measurements were carried out in a Magnetic Property Measurement System (MPMS-XL, Quantum Design) with standard d.c. techniques using a Keithley 6430 sub-femtoamp remote sourcemeter.

Received 20 January 2009; accepted 17 March 2009; published online 19 April 2009

## References


1. Beloborodov, I. S., Lopatin, A. V., Vinokur, V. M. & Efetov, K. B. Granular electronic systems. *Rev. Mod. Phys.* **79,** 469–518 (2007).
2. Murray, C. B., Kagan, C. R. & Bawendi, M. G. Synthesis and characterization of monodisperse nanocrystals and close-packed nanocrystal assemblies. *Ann. Rev. Mater. Sci.* **30,** 545–610 (2000).
3. Markovich, G. *et al.* Architectonic quantum dot solids. *Acc. Chem. Res.* **32,** 415–423 (1999).
4. Fan, H. Y. *et al.* Self-assembly of ordered, robust, three-dimensional gold nanocrystal/silica arrays. *Science* **304,** 567–571 (2004).
5. Bawendi, M. G., Steigerwald, M. L. & Brus, L. E. The quantum mechanics of larger semiconductor clusters (quantum dots). *Ann. Rev. Phys. Chem.* **41,** 477–496 (1990).
6. Alivisatos, A. P. Semiconductor clusters, nanocrystals and quantum dots. *Science* **271,** 933–937 (1996).
7. Xia, Y. N. *et al.* One-dimensional nanostructures: Synthesis, characterization and applications. *Adv. Mater.* **15,** 353–389 (2003).
8. Remacle, F. & Levine, R. D. Quantum dots as chemical building blocks: Elementary theoretical considerations. *ChemPhysChem* **2,** 20–36 (2001).
9. Chung, S. W., Markovich, G. & Heath, J. R. Fabrication and alignment of wires in two dimensions. *J. Phys. Chem. B* **102,** 6685–6687 (1998).
10. Bezryadin, A., Westervelt, R. M. & Tinkham, M. Self-assembled chains of graphitized carbon nanoparticles. *Appl. Phys. Lett.* **74,** 2699–2701 (1999).
11. Elteto, K., Lin, X. M. & Jaeger, H. M. Electronic transport in quasi-one-dimensional arrays of gold nanocrystals. *Phys. Rev. B* **71,** 205412 (2005).
12. Tang, Z. Y. & Kotov, N. A. One-dimensional assemblies of nanoparticles: Preparation, properties, and promise. *Adv. Mater.* **17,** 951–962 (2005).
13. Huang, J. X., Tao, A. R., Connor, S., He, R. R. & Yang, P. D. A general method for assembling single colloidal particle lines. *Nano Lett.* **6,** 524–529 (2006).
14. DeVries, G. A. *et al.* Divalent metal nanoparticles. *Science* **315,** 358–361 (2007).
15. Xia, Y. N., Yin, Y. D., Lu, Y. & McLellan, J. Template-assisted self-assembly of spherical colloids into complex and controllable structures. *Adv. Funct. Mater.* **13,** 907–918 (2003).
16. Cui, Y. *et al.* Integration of colloidal nanocrystals into lithographically patterned devices. *Nano Lett.* **4,** 1093–1098 (2004).
17. Kraus, T. *et al.* Nanoparticle printing with single-particle resolution. *Nature Nanotech.* **2,** 570–576 (2007).
18. Melosh, N. A. *et al.* Ultrahigh-density nanowire lattices and circuits. *Science* **300,** 112–115 (2003).
19. Zeng, H. *et al.* Magnetotransport of magnetite nanoparticle arrays. *Phys. Rev. B* **73,** 020402 (2006).
20. Yakimov, A. I. *et al.* Long-range Coulomb interaction in arrays of self-assembled quantum dots. *Phys. Rev. B* **61,** 10868–10876 (2000).
21. Beverly, K. C., Sampaio, J. F. & Heath, J. R. Effects of size dispersion disorder on the charge transport in self-assembled 2-D Ag nanoparticle arrays. *J. Phys. Chem. B* **106,** 2131–2135 (2002).
22. Yu, D., Wang, C. J., Wehrenberg, B. L. & Guyot-Sionnest, P. Variable range hopping conduction in semiconductor nanocrystal solids. *Phys. Rev. Lett.* **92,** 216802 (2004).
23. Zabet-Khosousi, A. & Dhirani, A. A. Charge transport in nanoparticle assemblies. *Chem. Rev.* **108,** 4072–4124 (2008).
24. Shklovskii, B. I. & Efros, A. L. in *Electronic Properties of Doped Semiconductors* (Springer, 1984).
25. Remacle, F., Beverly, K. C., Heath, J. R. & Levine, R. D. Conductivity of 2-D Ag quantum dot arrays: Computational study of the role of size and packing disorder at low temperatures. *J. Phys. Chem. B* **106,** 4116–4126 (2002).
26. Levin, E. I., Nguen, V. L., Shklovskii, B. I. & Efros, A. L. Coulomb gap and hopping electric conduction. Computer simulation. *Sov. Phys. JETP* **65,** 842–848 (1987).
27. Nguyen, V. D., Nguyen, V. L. & Dang, D. T. Variable range hopping in the Coulomb gap and gate screening in two dimensions. *Phys. Lett. A* **349,** 404–410 (2006).
28. Ancona, M. G. *et al.* Coulomb blockade in single-layer Au nanocluster films. *Phys. Rev. B* **64,** 033408 (2001).
29. Parthasarathy, R., Lin, X. M., Elteto, K., Rosenbaum, T. F. & Jaeger, H. M. Percolating through networks of random thresholds: Finite temperature electron tunneling in metal nanocrystal arrays. *Phys. Rev. Lett.* **92,** 076801 (2004).
30. Middleton, A. A. & Wingreen, N. S. Collective transport in arrays of small metallic dots. *Phys. Rev. Lett.* **71,** 3198–3201 (1993).
31. Elteto, K., Antonyan, E. G., Nguyen, T. T. & Jaeger, H. M. Model for the onset of transport in systems with distributed thresholds for conduction. *Phys. Rev. B* **71,** 064206 (2005).
32. Reichhardt, C. & Reichhardt, C. J. O. Temperature and a.c. effects on charge transport in arrays of metallic dots. *Phys. Rev. B* **68,** 165305 (2003).


## Acknowledgements

The authors would like to thank Peigen Cao and Yue Zou (Caltech) for helpful discussions and Xingchen Ye and C. B. Murray (University of Pennsylvania) for providing the gold quantum dots. This work was supported by the Department of Energy, the National Science Foundation, and the MARCO Center for Advanced Materials and Devices.

## Additional information

Supplementary information accompanies this paper at www.nature.com/naturenanotechnology. Reprints and permission information is available online at http://npg.nature.com/reprintsandpermissions/. Correspondence and requests for materials should be addressed to J.R.H.